

Full Length Article

Experimental and theoretical studies of the mechanism of oxidation of arsenopyrite in the presence of hydrogen peroxide

Kai Jiang^{a,b}, David Santos-Carballal^{b,c,*}, Jie Liu^a, Yuexin Han^a, Yimin Zhu^a, Yan Wang^a, Deju Zhang^{d,e,*}, Nora H. de Leeuw^{b,c}

^a College of Resource and Civil Engineering, Northeastern University, Shenyang 110819, China

^b School of Chemistry, Cardiff University, Main Building, Park Place, CF10 3AT Cardiff, UK

^c School of Chemistry, University of Leeds, Leeds LS2 9JT, UK

^d Biobank, Shenzhen Second People's Hospital, First Affiliated Hospital of Shenzhen University, Shenzhen 518035, People's Republic of China

^e National-Regional Key Technology Engineering Laboratory for Medical Ultrasound, Guangdong Key Laboratory for Biomedical Measurements and Ultrasound Imaging, School of Biomedical Engineering, Health Science Center, Shenzhen University, Shenzhen, China



ARTICLE INFO

Keywords:

Arsenopyrite
Oxidation
Surface characterization
Density functional theory

ABSTRACT

Arsenopyrite, which is a typical gold-bearing mineral, is widely distributed in gold tailings. In this study, we have examined the surface morphology of arsenopyrite before and after oxidation, the types of oxidation products, and the oxidation mechanism. We have carried out froth flotation and contact angle measurements and found that the wettability, which is a descriptor of the hydrophilicity of the arsenopyrite surfaces, increases with the levels of surface oxidation. X-ray photoelectron spectroscopy (XPS) was used to analyze the elemental composition before and after oxidation, which has demonstrated that both Fe(II) and As(III) oxidize to Fe(III) and As(V), respectively. The microscopic changes of the surface at the atomic level were also examined by atomic force microscopy (AFM), which indicated that the oxidation products gradually and partially cover the surface of the arsenopyrite upon reaction with hydrogen peroxide. These observations explain why the arsenopyrite XPS signal and the uniform change in wettability do not vanish completely during oxidation. Finally, density functional theory (DFT) calculations were used to describe the oxidation of the surface As atoms by the O of the chemisorbed hydrogen peroxide molecules. The computational results also show that the hydrogen peroxide dissociates into two hydroxyl groups that coordinate the Fe and As atoms on the surface of the arsenopyrite. The results of this study have important implications for the reuse of gold tailings containing arsenopyrite.

1. Introduction

With the rising demand for gold across all industries, the quality of basic ore deposits has gradually declined. Gold grades have currently reached 3–4 g/t and are predicted to fall to just 1 g/t by 2050, as a result of the depletion over time of the main high-quality gold ore deposits [1,2]. The extraction and sorting of gold unavoidably produces a significant number of by-products, known as gold tailings, which are dumped close to the mine site and take up valuable land resource [3,4]. As more gold ore is being mined, more gold tailings are also being produced. For example, China alone has been generating 24.5 million

tons of gold tailings annually [5,6]. In situ storage, which is the most common method for treating gold tailings, uses a lot of arable land, whereas the oxidation of the sulfides in the tailings produces acidic mine wastewater, which is extremely harmful to human health and the environment [7,8]. Moreover, gold tailings still contain a significant amount of recoverable gold, silver, and other metals, making them an incredibly valuable secondary resource [9]. The prudent utilisation of gold tailings can assist with resource recycling, while also contributing to environmental conservation.

Arsenopyrite-containing gold ore is frequently found in basic gold deposits and is typically hard to treat [10]. The arsenopyrite mineral

* Corresponding authors at: School of Chemistry, University of Leeds, Woodhouse Lane, Leeds, West Yorkshire LS2 9JT, United Kingdom (D. Santos-Carballal); Biobank, Shenzhen Second People's Hospital, First Affiliated Hospital of Shenzhen University, Shenzhen 518035, People's Republic of China; National-Regional Key Technology Engineering Laboratory for Medical Ultrasound, Guangdong Key Laboratory for Biomedical Measurements and Ultrasound Imaging, School of Biomedical Engineering, Health Science Center, Shenzhen University, Shenzhen, China (D. Zhang).

E-mail addresses: D.Santos-Carballal@leeds.ac.uk (D. Santos-Carballal), u3005757@connect.hku.hk (D. Zhang).

<https://doi.org/10.1016/j.apsusc.2023.157673>

Received 10 April 2023; Accepted 31 May 2023

Available online 10 June 2023

0169-4332/© 2023 The Authors. Published by Elsevier B.V. This is an open access article under the CC BY license (<http://creativecommons.org/licenses/by/4.0/>).

surrounds the gold particles in the ore, and because of the dense structure of the host, any leaching agent cannot effectively get into contact with the gold particles, thereby lowering the recovery efficiency of the precious metal [11,12], which ultimately is retained in the tailings. In the past, the gold grade in these arsenic-bearing gold tailings was even larger than in most current ore deposits, [13] because of the low efficiency or inadequate separation techniques available at the time. However, even now it is beneficial to analyze and utilize these because, despite the presence of arsenic, they contain significant valuable residue.

Arsenopyrite encapsulating gold particles will unavoidably be subjected to weathering during the stockpiling process, creating diverse oxidation products [14]. These oxidation by-products, which primarily consist of insoluble carbonates and arsenates as well as hydroxy-iron compounds, create loose and unstable hardpans on the surface of the mineral [15], thereby facilitating subsequent oxidation [16]. As a result, as the arsenopyrite oxidises, it breaks down and releases the gold over a prolonged period of weathering. This process enables the efficient leaching and recovery of gold without the need for expensive pre-treatment that would otherwise be costly due to arsenopyrite encapsulation. As such, research on the various stages of oxidation of arsenopyrite is crucial to gain insight into the exposure of the gold particles from the arsenic-bearing gold tailings. Prior research on the oxidation of arsenopyrite has largely concentrated on the release of Fe(III) and the oxidation of arsenopyrite by oxygen in air [10,17]. In an acidic environment, the Fe(II) in arsenopyrite is initially oxidized to Fe(III), followed by the oxidation of AsS_2^- to As(III) and SO_4^{2-} , and the slow oxidation of As(III) to As(V) by oxygen [18–20]. However, since the tailings are stacked outdoors, ultraviolet (UV) light plays a significant role in the oxidation of arsenopyrite, as earlier research has shown [21]. Eqs. (1)–(3) describe the chemical reactions for the oxidation of As(III) by oxygen from air under UV light, which involves dissolution of As(III) and formation of the O_2^- and HO_2^- radicals. These radicals will then react to form H_2O_2 (Eq. (4), (5)) [22]. H_2O_2 is clearly a better oxidizing agent than O_2 and Fe(III), hence it has paramount importance in the entire process of arsenopyrite oxidation in open pits. However, it is still unclear how H_2O_2 affects the oxidation process and morphology of arsenopyrite.



The potential impact of H_2O_2 in the release of gold particles that are encased within the arsenopyrite host have led us to study the oxidation of this mineral phase using experimental and computational techniques. In order to examine the recovery of arsenopyrite following oxidation by various concentrations of H_2O_2 , flotation tests were used, which is a method frequently used in the mineral processing industry to separate and enrich minerals. Atomic force microscopy (AFM) was used to study the surface morphological changes of arsenopyrite at various levels of oxidation. By using X-ray photoelectron spectroscopy (XPS) mapping, the elemental composition of the oxidized arsenopyrite surface and the corresponding chemical elements were determined. Finally, computer simulations based on the density functional theory (DFT) were employed to confirm the structure, energy, charge transfer, and electronic configuration of H_2O_2 adsorbed on the surface of arsenopyrite. The outcomes of these experiments and theoretical calculations provide fundamental insight to support the resource exploitation of arsenic-containing gold tailings.

2. Materials and methods

2.1. Materials and reagents

The arsenopyrite mineral samples were collected from Guilin, Guangxi, China. Arsenopyrite samples were first hand-selected for good crystallinity and purity, crushed in an agate mortar, and dry sieved using a 74 μm sieve. The off-sieve fraction was collected and washed three times with anhydrous ethanol to remove the ultra-fine powder. The washed samples were vacuum dried and stored for further analysis. The chemical composition of the arsenopyrite samples was determined by inductively coupled plasma (ICP) spectrometry and the results showed that the tested material was 34.20% Fe, 44.80% As and 20.1% S, indicating 97.39% purity of FeAsS. X-ray diffraction (XRD) results showed that all samples had the arsenopyrite phase and good crystallinity. The oxidation of arsenopyrite was tested as follows. Each time 2 g of arsenopyrite sample was placed in a 30 ml stirring tank and 20 ml of deionised water was added. After adjusting the solution to pH = 3, the corresponding concentration of H_2O_2 solution was added and the sample was stirred for 3 min before filtering and drying under vacuum. All the chemicals used were analytically pure (Sinopharm Chemical Reagent Co., Ltd.) and deionised water (18.2 $\text{M}\Omega\text{-cm}$) was used in the experiments.

2.2. Micro-flotation experiments

The flotation experiments were carried out using an XFG-II laboratory flotation machine (Jilin Exploration Machinery Factory, China). 2 g of arsenopyrite sample with 20 ml of deionised water was added to a 30 ml flotation tank at 1800 rpm for each flotation measurement. After the pulp stabilised, the pH was adjusted to an appropriate value by adding HCl and NaOH, followed by the addition of sodium butyl xanthate and stirring for 3 min. The froth product and tailings were collected, filtered, vacuum dried and weighed to calculate the recovery. Three flotation tests were carried out under each condition and the results were averaged to give the final flotation recovery.

2.3. Wettability measurements

Wettability measurements on arsenopyrite surfaces were made using a contact angle meter, model JC2000C. Before each treatment with different concentrations of hydrogen peroxide, the arsenopyrite surface was polished with a polishing agent to eliminate the effect of surface roughness and oxidation prior to carrying out the contact angle measurements. The polished arsenopyrite slices were immersed in the hydrogen peroxide solution with the appropriate concentration for 3 min, which was followed by rinsing with deionised water and vacuum drying. For each measurement, a 6 μl droplet of deionised water was placed on the arsenopyrite surface using a micro-syringe and a high-speed camera was used to film the droplet touching the surface as well as the stabilisation process. The contact angle experiments were performed using a five-point method, with three values measured at a time and averaged as the final result.

2.4. Atomic force microscopy (AFM) imaging

The surface morphology of arsenopyrite was obtained using a MultiMode 8.0 AFM (Bruker, USA). Arsenopyrite sample pieces with freshly created surfaces and atomic-level smoothness were used as test substrates. The cantilever of the test probe (SNL-10, Bruker, USA) ended in a Si_3N_4 tip with a resonance frequency of 65 kHz and a spring constant of 0.35 N/m. After imaging the natural arsenopyrite substrate, it was immersed in H_2O_2 solution at an appropriate concentration and pH for 3 min. Since the flotation data demonstrated that the pH range between 4 and 10 has a greater impact on arsenopyrite flotation recovery, we have chosen a final intermediate pH value of 7.0. All images were acquired in

air using a tapping mode and processed by Nanoscope Analysis v1.8 software. The depth of colour in the AFM images quantifies the high morphological fluctuations of the mineral surface.

2.5. X-ray photoelectron spectroscopy analysis

VersaProbe II (ULVAC-PHI, Japan) was used for the XPS test, and a 200-W monochromatic Al K X-ray source (1486.7 eV) was used under chamber vacuum conditions (vacuum pressure less than 110^{-6} Pa). During the investigation, an unidentified carbon C 1s peak with a binding energy of 284.8 eV was used to calibrate all the elements. The final data were analyzed with MultiPak software, and the Fe 2p_{3/2}, As 3d_{5/2}, and S 2p_{3/2} peaks were fitted with narrow scan spectra using the Gauss-Lorentz method.

2.6. Computational details

The surface structure of arsenopyrite and the adsorbed species were optimized using the Vienna Ab initio Simulation Package (VASP), which is based on the plane wave density functional theory (PW-DFT) [23,24]. The interaction between ion nuclei and valence electrons was described using the projected augmented wave (PAW) approach, and the electron exchange-correlation energy was calculated using the Perdew Burke Ernzerhof (PBE) generalized gradient approximation (GGA) functional [25,26]. The Grimme D3 method was utilized in all computations to account for the long-range Van der Waals dispersion interactions in the structures [27,28]. Test calculations showed that the energy of the optimized system can converge to within 10^{-6} eV when the cutoff energy is 400 eV, whereas the Hellman-Feynman forces converged to within 0.01 eV/Å. A Monkhorst Pack mesh of $2 \times 2 \times 1$ k-points was used to model the surface and adsorption structures.

We have used the METADISE code[29] to cut the optimised crystal structure of arsenopyrite and create its (001) surface. The surface created by METADISE ensures that the dipole moment perpendicular to the surface plane is zero. A 12 Å vacuum gap is placed above the top atom in the surface to avoid interaction with the periodic images.

Different initial H₂O₂ adsorption modes, e.g. various hydrogen and oxygen atom orientations and configurations, were fully optimised. The most stable adsorption structures were utilized to establish if the adsorption of H₂O₂ on the arsenopyrite surface can take place. The adsorption energy (E_{ads}) of H₂O₂ on the arsenopyrite surface was calculated as:

$$E_{\text{ads}} = E_{\text{Surface+mol}} - E_{\text{Surface}} - E_{\text{mol}} \quad (6)$$

where E_{mol} is the energy of the hydrogen peroxide molecule, and $E_{\text{Surface+mol}}$ and E_{Surface} are the energies of the combined H₂O₂-FeAsS system and the pure surface, respectively. As such, exothermic reactions and spontaneous adsorption processes lead to negative values of the adsorption energy.

3. Results and discussion

3.1. Flotation recovery

Fig. 1 illustrates how pH and H₂O₂ concentration affect arsenopyrite flotation recovery in a system with sodium butyl xanthate acting as a trap. As can be observed, the flotation recovery of arsenopyrite under acidic conditions, i.e. pH = 2, was significant in the absence of H₂O₂. Note that an equal volume of deionized water was added to maintain similar experimental conditions. The recovery reduced as the pH rose to 4, but at pH = 6, the recovery increased to 60 %, although for pH > 6, we found that the total recovery declined. The general flotation pattern of arsenopyrite was disrupted by the addition of H₂O₂, and the overall recovery decreased with pH. If the H₂O₂ concentration rises further, arsenopyrite recovery at each pH tends to steadily decline, which shows

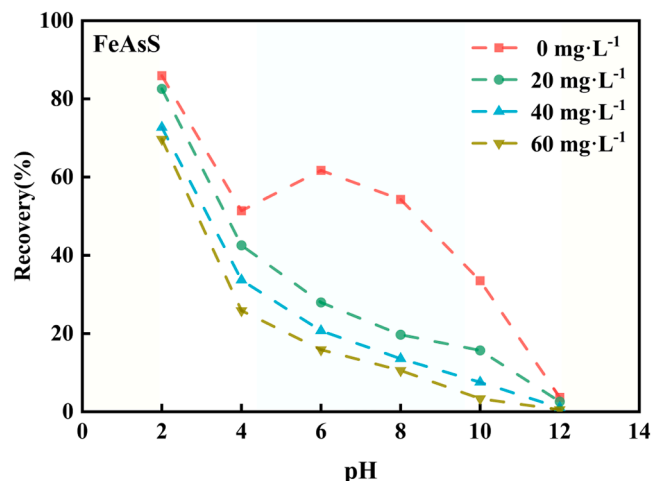


Fig. 1. Flotation recovery of arsenopyrite as a function of pH and H₂O₂ concentration when sodium butyl xanthate is the collector and methyl isobutyl carbinol is the frother (SBX = 60 mg·L⁻¹, MIBC = 20 mg·L⁻¹).

that arsenopyrite is inhibited by the oxidation of H₂O₂.

The floatability of arsenopyrite was relatively large at all H₂O₂ concentrations for pH = 2, since the majority of the oxidation products under acidic conditions were primarily in the form of hydrophobic iron ions. After the pH increased to 4, it was evident that the flotation curves in the presence of H₂O₂ were significantly inhibited compared to the experiments in the absence of H₂O₂. We found that the hydroxyl iron species, which concentration rises in solution with pH, adsorb on the mineral surface, thereby increasing the hydrophilicity of the surfaces and inhibiting flotation of the material.

3.2. Surface wettability

The contact angle is an important parameter in froth flotation, as it measures the wettability of the solid surface, which describes the hydrophilicity or hydrophobicity of the mineral surface. As can be seen from Fig. 2, the contact angle of the natural arsenopyrite surface before interaction with H₂O₂ is 70.9°, which indicates the naturally hydrophobic character of this material. When the surface of arsenopyrite was treated with 20 mg·L⁻¹ of H₂O₂, the contact angle decreased to 47.5°, indicating oxidation of the mineral surface and an increase of hydrophilicity. When the H₂O₂ concentration was increased to 60 mg·L⁻¹, the

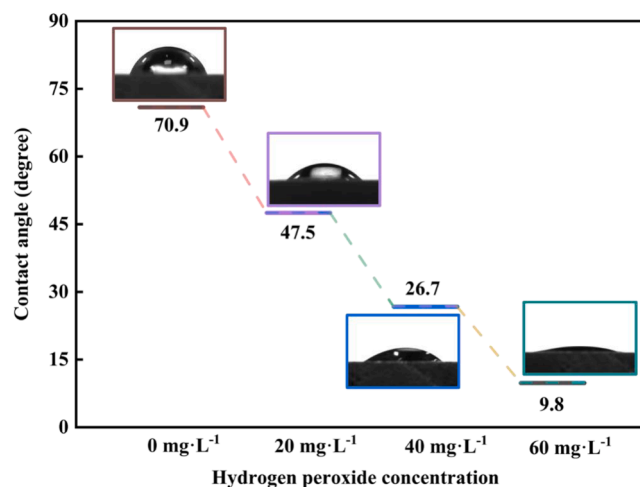


Fig. 2. Variation in contact angle of arsenopyrite at different H₂O₂ concentrations.

contact angle was further reduced to 9.8° and the surface became fully hydrophilic. The results of the microbubble flotation tests are also compatible with these findings, as they show that when the concentration of H_2O_2 rises, the oxidation of the arsenopyrite surface progressively increases, leading to the gradual accumulation of hydrophilic species at the surface and the reduction of the floatability of the material. These findings demonstrate that hydrogen peroxide also alters the floatability of the system by modifying the wettability of the arsenopyrite surface.

3.3. Surface morphology

Fig. 3 shows the surface of arsenopyrite before and after being submerged in solutions with different concentrations of H_2O_2 . In order to discuss the distribution and accumulation of oxidation products on the mineral surface, the 3D morphologies show the average height and root-mean-square (RMS) surface roughness. Fig. 3 also illustrates the effect of the degree of oxidation on the surface morphology of arsenopyrite.

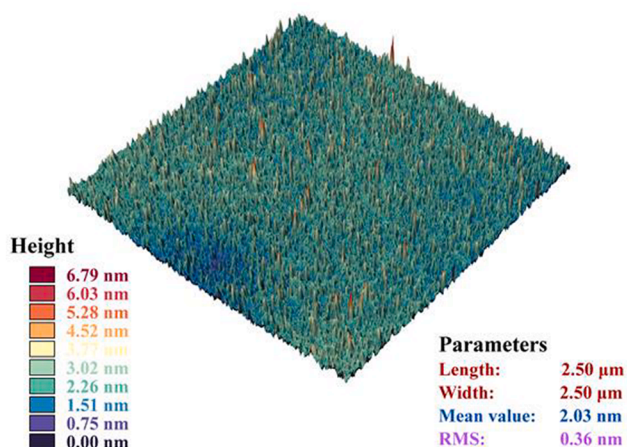
As seen in Fig. 3(a), the surface of a natural arsenopyrite sample was examined using atomic force microscopy before oxidation, in order to use it as a reference in comparisons with the surface morphology after oxidation by H_2O_2 . Because there are no impurities or crystal flaws on the surface of natural, non-oxidized arsenopyrite, it is evident that the surface is essentially flat and there are no significant areas of unevenness. We found that the average height of the surface was 2.03 nm, and

the roughness was 0.36 nm for the pristine material.

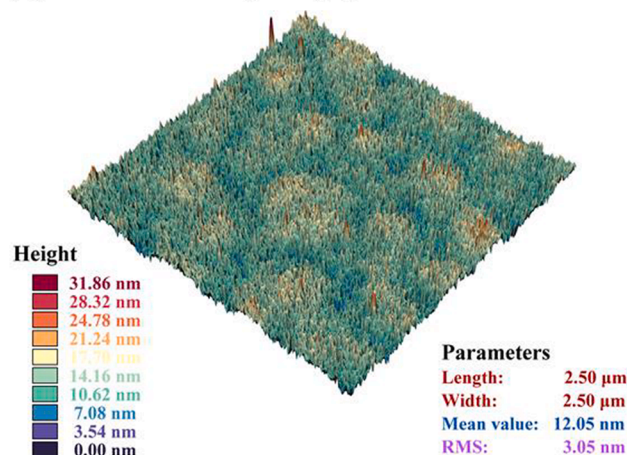
Arsenopyrite begins to evenly show convex patches on its surface after 30 min of soaking in a $20 \text{ mg}\cdot\text{L}^{-1}$ H_2O_2 solution (Fig. 3(b)). The development and buildup of surface oxidation products is the primary cause of this observation, and the shape of the protrusion is primarily determined by the crystal structure. The result of surface wettability is consistent with this shift in surface morphology. The oxidation experiments were carried out at $\text{pH} = 7$, which led to the adsorption of a large concentration of hydrophilic species onto the arsenopyrite surface. The surface becomes covered with the newly formed hydrophilic oxidation products, thereby increasing its wettability. In contrast to the natural, unoxidized arsenopyrite surface, the average height of the surface after oxidation using the H_2O_2 solution with a concentration of $20 \text{ mg}\cdot\text{L}^{-1}$ is 12.05 nm, and the surface roughness is 3.05 nm.

As anticipated, when the concentration of the H_2O_2 solution is increased to 40 and $60 \text{ mg}\cdot\text{L}^{-1}$, the oxidized arsenopyrite surface exhibits an increased protrusion area, larger protrusion height surface, and rougher overall surface (Fig. 3(c) and (d)), mainly caused by the accumulation of additional oxygenated products and the consequent expansion of the surface reaction area. The average height and roughness of the arsenopyrite surface increased after oxidation to 18.44 and 22.28 nm, for H_2O_2 concentrations 40 and $60 \text{ mg}\cdot\text{L}^{-1}$ respectively, while the roughness was 4.42 and 4.78 nm. The results also show that the oxidation products gradually grow and accumulate on areas with surface defects, increasing the wettability of arsenopyrite.

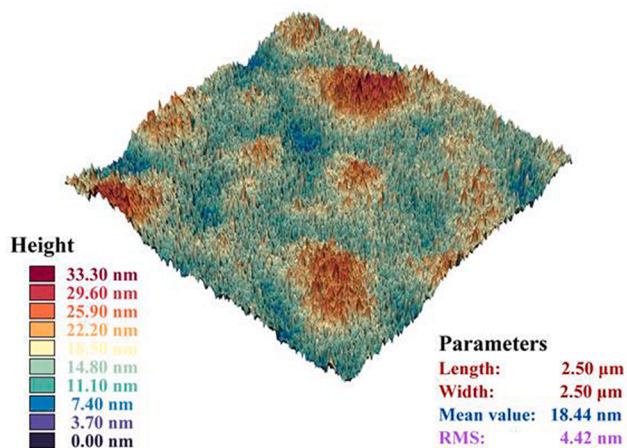
(A) Natural



(B) Oxidized with $20 \text{ mg}\cdot\text{L}^{-1}$ H_2O_2



(C) Oxidized with $40 \text{ mg}\cdot\text{L}^{-1}$ H_2O_2



(D) Oxidized with $60 \text{ mg}\cdot\text{L}^{-1}$ H_2O_2

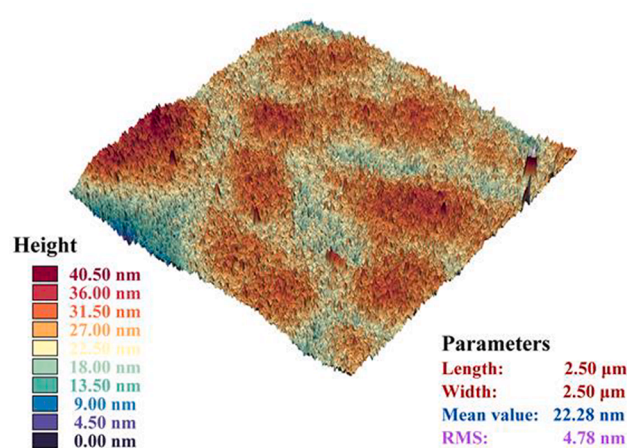


Fig. 3. AFM 3D images of arsenopyrite surfaces under different conditions. (a) Natural arsenopyrite surface; (b) $20 \text{ mg}\cdot\text{L}^{-1}$ H_2O_2 -impregnated arsenopyrite; (c) $40 \text{ mg}\cdot\text{L}^{-1}$ H_2O_2 -impregnated arsenopyrite; (d) $60 \text{ mg}\cdot\text{L}^{-1}$ H_2O_2 -impregnated arsenopyrite.

3.4. High-resolution XPS

XPS was used to examine the oxidation products on the surface of the arsenopyrite in solutions containing various concentrations of hydrogen peroxide. In order to calculate the chemical states and relative concentrations of the elements on the surface of oxidised arsenopyrite, the binding energy of each element was determined by fitting their spectra. Figs. 4-6 display the high-resolution XPS spectral peak position fitting, and Table 1 lists the calculated relative contents of each chemical element.

First, as can be seen in Fig. 4, the Fe 2p_{3/2} signals were primarily matched to two recognizable peaks with binding energies that were situated at 707.08 and 711.17 eV, respectively. It is possible to infer that only the low spin Fe(II) state, which displays a single peak at 707.08 eV corresponding to the chemical state of Fe in unoxidized arsenopyrite, is present on the mineral surfaces [30,31]. With rising H₂O₂ concentration, the peak in arsenopyrite corresponding to Fe(II) steadily declines. In contrast, the peak at 711.17 eV is caused by the Fe(III) ion resulting from the oxidation of the arsenopyrite surface [32,33], which rises with an increase in H₂O₂ concentration, and the formation of Fe oxides.

After oxidation, the As 3d spectra (Fig. 5) are primarily split into three peaks, with binding energies of 41.22, 43.77, and 45.06 eV for the 3d_{5/2} level, characteristic of As⁻¹-S⁻¹ [30-32,34], As³⁺-O, and As⁵⁺-O groups, respectively [35-37]. As⁻¹-S is the chemical state of As in arsenopyrite in the absence of oxidation. When arsenopyrite starts to oxidize, the oxide species gradually accumulate and cover its surface, as shown by the two chemical states of As³⁺-O and As⁵⁺-O appearing with an increase of H₂O₂ concentration. The relative content of As³⁺-O was larger than the more oxidized As⁵⁺-O state prevalent in low concentrations of H₂O₂, confirming that the former species was formed during the initial phase of surface oxidation. We found that arsenopyrite content on the surface declines dramatically with the H₂O₂ concentration, as As⁻¹ becomes oxidised.

Fig. 6 displays the results of peak fitting of the S 2p spectra after the surface of the arsenopyrite was oxidized. Two peaks of the S 2p_{3/2}

spectrum, with binding energies of 162.25 and 168.17 eV, correspond to the chemical states AsS²⁻ and SO₄²⁻, which is a post-oxidized state [31,33,38], where AsS²⁻ denotes the chemical state of S atoms in arsenopyrite [30,35,37]. The relative content of AsS²⁻ noticeably decreases with increasing H₂O₂ concentration because of the accumulation and coverage of oxidation products on the surface, whereas the relative content of SO₄²⁻ gradually increases with H₂O₂ concentration, denoting the accelerated oxidation of elemental S. The XPS results for all the arsenopyrite elements demonstrate that deep oxidation cannot shield the elemental detection signal of this mineral. Note that, as demonstrated by the AFM experiments, the distribution and thickness of oxidation products cannot be greater than the detection range of XPS. However, both, XPS and AFM show that as H₂O₂ concentration rises, the degree of oxidation of the arsenopyrite surface deepens, as the height and roughness of the AFM image increases. This change in the surface structure causes a reduction in the amount of exposed elements of arsenopyrite detected by our XPS experiments and an increase in the number of hydrophilic species available on the surface of the mineral, which is also consistent with the wettability results.

3.5. Adsorption of hydrogen peroxide

3.5.1. Adsorption structures

Density functional theory calculations were used to calculate the adsorption energies, bond lengths, and electron change transfers before and after adsorption of hydrogen peroxide on the As, S, and Fe sites of the (001) surface of arsenopyrite. The most stable configurations are shown in Fig. 7 and the electron transfers as well as the adsorption energies are shown in Table 2.

First, the orientation of the H-atoms in hydrogen peroxide has a significant impact on the adsorption energy. The results clearly show that an H-atom facing downward is not favorable for overall adsorption, with the adsorption energy ranging from -33.77 to -26.05 kJ/mol. In contrast, when the H-atom is facing upward, the O in hydrogen peroxide directly interacts with the As and S atoms on the surface of arsenopyrite,

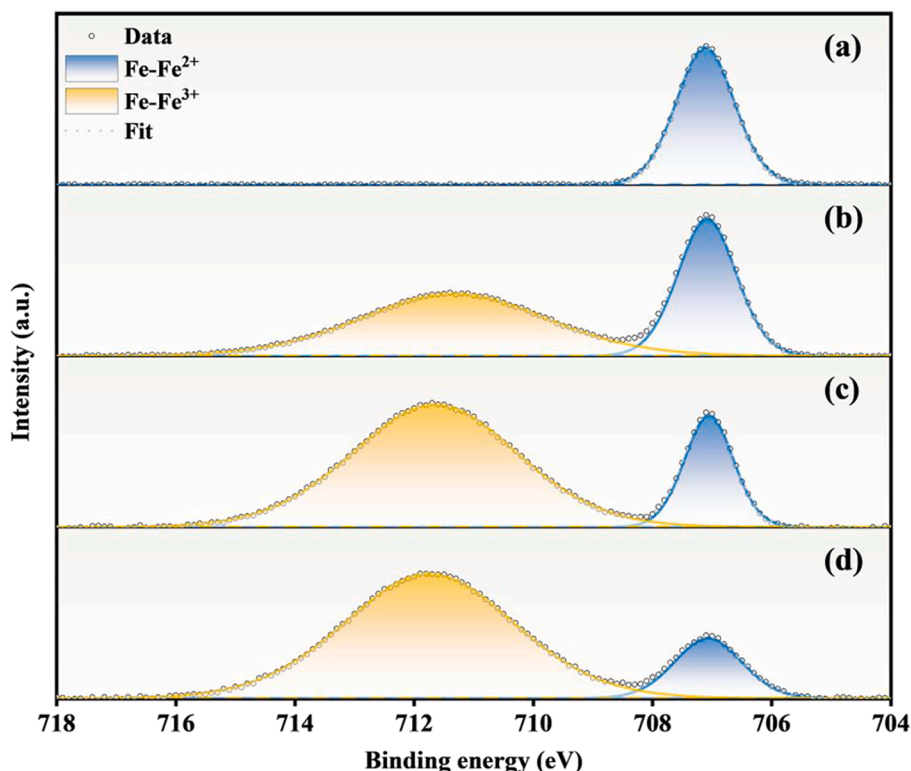


Fig. 4. Fe 2p_{3/2} spectra of arsenopyrite after oxidation for H₂O₂ concentrations of: (a) 20 mg·L⁻¹, (b) 40 mg·L⁻¹ and (c) 60 mg·L⁻¹.

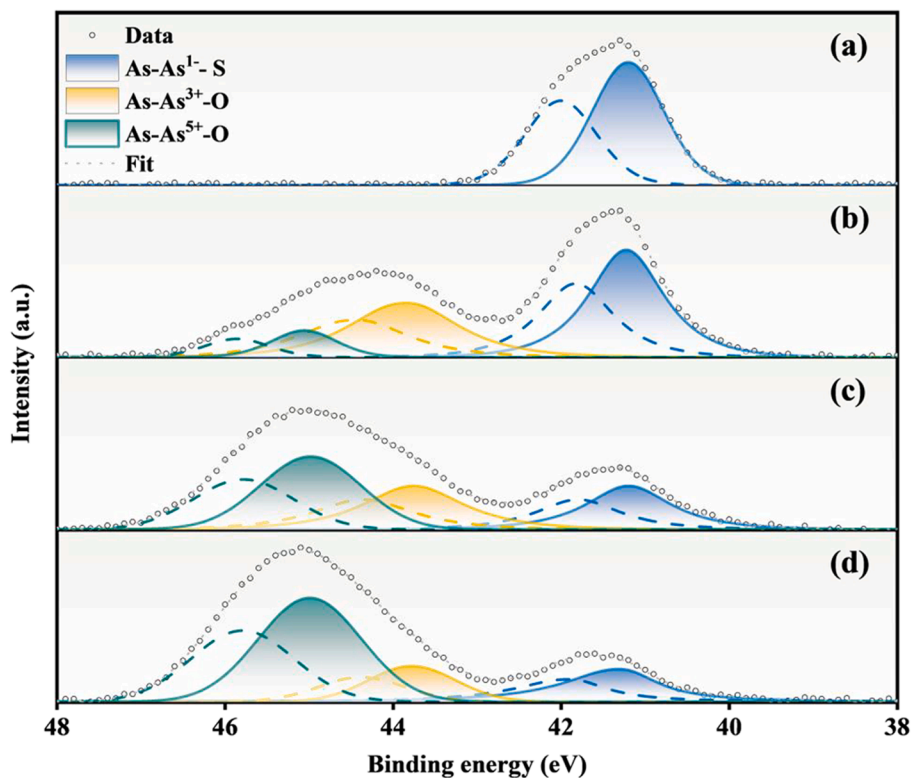


Fig. 5. As 3d spectra of arsenopyrite after oxidation for H_2O_2 concentrations of: (a) $20 \text{ mg}\cdot\text{L}^{-1}$, (b) $40 \text{ mg}\cdot\text{L}^{-1}$ and (c) $60 \text{ mg}\cdot\text{L}^{-1}$.

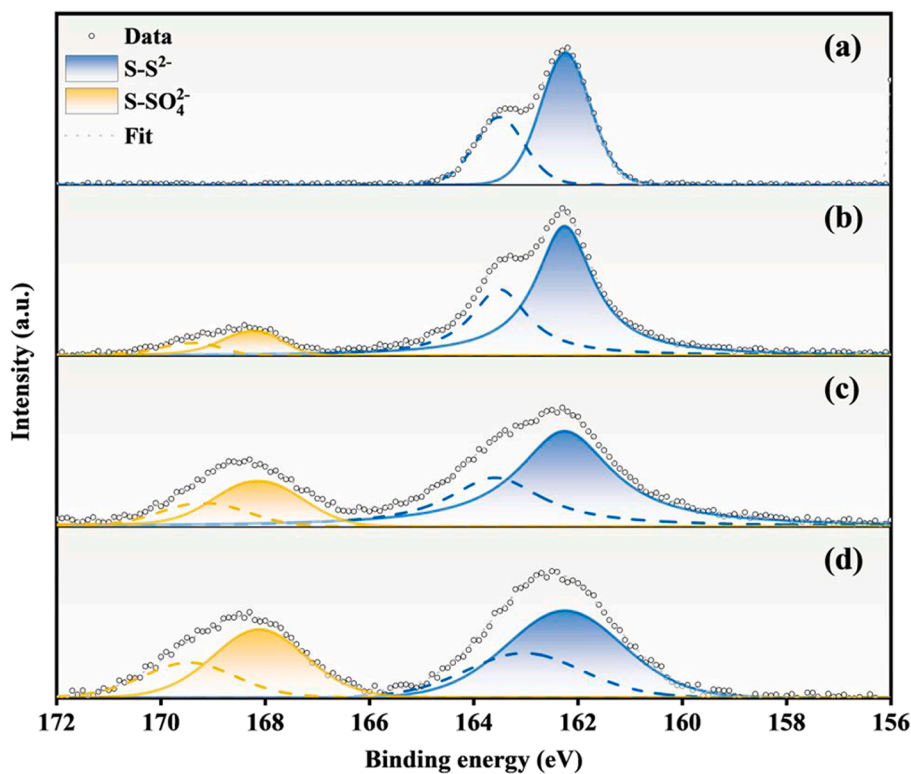


Fig. 6. S 2p spectra of arsenopyrite after oxidation for H_2O_2 concentrations of: (a) $20 \text{ mg}\cdot\text{L}^{-1}$, (b) $40 \text{ mg}\cdot\text{L}^{-1}$ and (c) $60 \text{ mg}\cdot\text{L}^{-1}$.

and the adsorption energy ranges from -368.57 to -254.72 kJ/mol. Consequently, it is evident from the binding energies that strong hydrogen peroxide adsorption only takes place when the adsorbate O

atoms can coordinate directly to the surface atoms. However, only weak physisorption occurs when the H-atom is directly interacting with the surface.

Table 1

Relative contents of Fe 2p_{3/2}, As 3d_{5/2} and S 2p_{3/2} on the surface of arsenopyrite after oxidation.

| Element | Binding energy | Chemical state | Relative intensity (%) | | | |
|---------|----------------|-------------------------------|------------------------|-----------------------|-----------------------|-----------------------|
| | | | 0 mg·L ⁻¹ | 20 mg·L ⁻¹ | 40 mg·L ⁻¹ | 60 mg·L ⁻¹ |
| Fe | 707.08 | Fe ²⁺ -AsS | 100.00 | 40.83 | 21.26 | 15.97 |
| | 711.17 | Fe ³⁺ -O | 0.00 | 59.17 | 78.74 | 84.03 |
| As | 41.22 | As ¹⁻ -S | 100.00 | 52.36 | 25.89 | 23.21 |
| | 43.77 | As ³⁺ -O | 0.00 | 36.65 | 29.46 | 17.26 |
| | 45.06 | As ⁵⁺ -O | 0.00 | 10.99 | 44.65 | 59.53 |
| S | 162.25 | AsS ²⁻ | 100.00 | 86.96 | 74.07 | 61.35 |
| | 168.17 | SO ₄ ²⁻ | 0.00 | 13.04 | 25.93 | 38.65 |

Additionally, as seen in Fig. 7(a), hydrogen peroxide forms two As-O bonds with bond lengths of 1.84 and 1.92 Å on the surface of arsenopyrite, where it is adsorbed to the same As atom as two hydroxyl groups. We found that the adsorption energy was -254.73 kJ/mol in this adsorption mode. It is observed that hydrogen peroxide also dissociates into two hydroxyl groups over the surface S atom, which is consistent with previous reports [39]. We tested the adsorption of H₂O₂ at the S site, but found that the molecule indeed dissociates and the O atoms prefer to coordinate two nearby As atoms, with bond lengths of 1.84 and 1.81 Å (Fig. 7(c)). Despite the fact that the two O species were bound to two separate As atoms, it was clear that the As₂-O₁ bond length was shorter than when the OH groups adsorb at the same As atom. As a result, the adsorption energy was -368.57 kJ/mol at nearby As sites, which was higher than the value calculated at the same As site, and it follows that arsenopyrite has a greater affinity for H₂O₂ adsorbing on two nearby As atoms than to the same As atom. At the Fe site, the adsorbed H₂O₂ will again dissociate into two hydroxyl fragments Fig. 7(e). Upon interaction with the mineral surface, the two hydroxyl groups form Fe-O and As-O bonds, releasing a total adsorption energy of -314.54 kJ/mol. The bond length of the As-O bond (1.78 Å) was shorter than the As-O bond at the two previous sites, i.e. one As and two nearby

As atoms. However, the presence of the Fe-OH species caused an overall weaker adsorption energy than for two nearby As-OH species, explaining the intermediate adsorption energy calculated for this interaction. However, bonding to two different atoms always led to a higher adsorption energy than bonding to a single atom. The adsorption energy at the Fe site was still higher than at a single As site.

3.5.2. Electronic properties

In order to describe the electronic properties of the adsorption systems, the atomic charge transfers have been calculated [40,41], see Table 2. When a single As atom is bound by two OH groups (Fig. 7(a)), the surface As₁ atom loses 0.80 electrons (e⁻) during adsorption, demonstrating oxidation of As(III) to As(V), while the nearby As atom, despite not being a direct participant in the reaction, still loses 0.12 e⁻, demonstrating a slight overall oxidation on the surface of the arsenopyrite. The O atoms from the OH fragments gained 0.53 and 0.58 e⁻, indicating that they were the main oxidizing agent, reducing their oxidation number from -1 to -2. The results after adsorption at two nearby As sites showed that the two O atoms from the OH fragments also received 0.53 and 0.58 e⁻ upon adsorption (Fig. 7(c)), proving that the

Table 2

Adsorption energy (E_{ads}) of H₂O₂ on the FeAsS(001) surface and charge transfers (Δq) of As, S and Fe atoms on the surface of arsenopyrite before and after hydrogen peroxide adsorption (A positive charge difference indicates that the adsorption site gains electrons).

| | O ₁ | O ₂ | As ₁ | As ₂ | Fe ₁ | $E_{\text{ads}}/\text{kJ}\cdot\text{mol}^{-1}$ |
|-----|----------------|----------------|-----------------|-----------------|-----------------|--|
| | $\Delta q/e^-$ | $\Delta q/e^-$ | $\Delta q/e^-$ | $\Delta q/e^-$ | $\Delta q/e^-$ | |
| (a) | 0.53 | 0.58 | -0.80 | -0.12 | -0.03 | -254.72 |
| (b) | -0.01 | 0.00 | -0.12 | 0.01 | 0.00 | -26.05 |
| (c) | 0.53 | 0.58 | -0.54 | -0.56 | 0.00 | -368.57 |
| (d) | 0.02 | -0.02 | -0.01 | -0.08 | 0.01 | -27.02 |
| (e) | 0.51 | 0.54 | -0.62 | 0.01 | -0.21 | -314.54 |
| (f) | 0.02 | 0.02 | -0.10 | -0.02 | 0.01 | -33.77 |

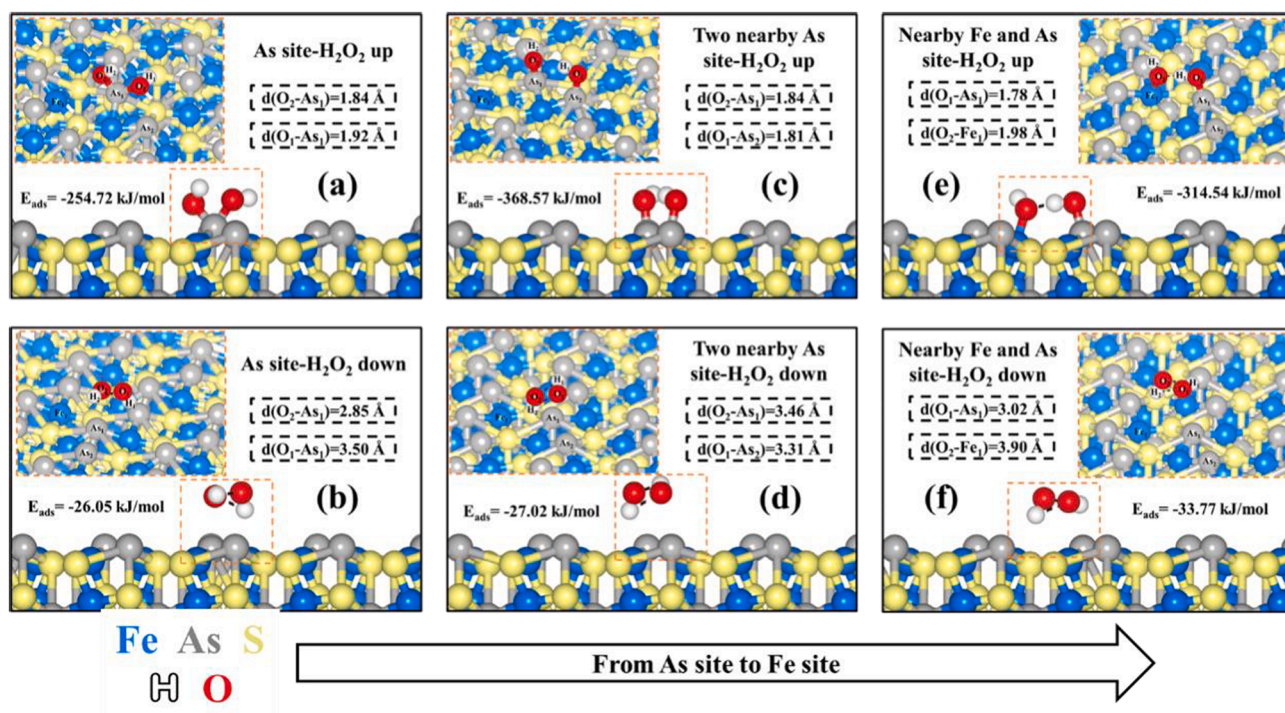


Fig. 7. Geometric configuration of the arsenopyrite surface after hydrogen peroxide adsorption: (a) H up for H₂O₂ on a single As site, (b) H down for H₂O₂ on a single As site, (c) H up for H₂O₂ on two nearby As sites, (d) H down for H₂O₂ on two nearby As sites, (e) H up for H₂O₂ on nearby Fe and As site, (f) H down for H₂O₂ on nearby Fe and As site.

O atoms underwent similar electron transfers during the oxidation processes at a single and two nearby As sites. The As_1 and As_2 atoms, on the other hand, lose 0.54 and 0.56 e^- , respectively, demonstrating that they become equally oxidized. However, the total charge transferred from the two As atoms is higher after adsorption at two nearby As sites ($-1.10 e^-$) than at the single As site ($-0.92 e^-$), since the OH groups can draw more charge from separate As atoms than from a single one. As_1 and Fe_1 lose 0.62 and 0.21 e^- , respectively, when the two OH fragments interact with the surface Fe site (Fig. 7(e)). Similar to the oxidation of the As(III) atoms to As(V) due to the loss of electrons, the Fe atom also oxidizes, becoming Fe(III). The As_1 atom loses the largest charge, since it has larger electronegativity than Fe. The formation of the Fe-O bonds leads to an overall adsorption energy that is intermediate between the energy released upon adsorption at two nearby As sites and at a single As site.

So far, our discussion have been centred on adsorption modes where the H_2O_2 molecule dissociates into two OH fragments, whereby an O atom is directly interacting with the surface of the arsenopyrite. We also found physisorption modes, where the H atom was bound to the surface, see Fig. 7(b), (d), and (f). For these physisorption modes, the atomic electron transfers are negligible, with the exception of the modest oxidation of the As atom, which loses 0.08–0.12 e^- . This supports our observation that low adsorption energies between -26.05 and -33.77 $\text{kJ}\cdot\text{mol}^{-1}$ are also connected to only minor surface oxidation processes occurring during these physisorption modes.

In order to shed light on the nature of the interaction between the H_2O_2 molecule and the arsenopyrite surface, the projected density of states (PDOS) of the atoms involved in the adsorption are displayed in Figs. 8–10. It can be seen in the PDOS of the free H_2O_2 prior to adsorption and of the exposed atoms on the arsenopyrite surface, that the region around the Fermi energy level is dominated by p states from the lone pair electron density of the anions. As a result, these orbitals are anticipated to interact strongly during adsorption of the H_2O_2 molecule with the mineral surface.

After adsorption on the As sites, we discovered that the O atoms of H_2O_2 interact with the p states of the surface As ions, which vanished or reduced the O-p states around the Fermi level, as shown in Fig. 8. However, the energy level and PDOS of the As-p state was altered visibly after adsorption, indicating intense hybridization between the O and the As_1 atoms. Note that, since there is no adsorption on the As_2 and Fe_1

atoms, the electronic properties of these ions are largely unaltered. H_2O_2 is stable through physical adsorption at this stage because the H atom in contact with the surface only undergoes a transition to energy levels below the O-p state, while the electronic densities of the other relevant atoms remain essentially unchanged [42].

The O-p state close to the Fermi energy level disappears or decreases when the OH fragments adsorb at the nearby As sites, indicating strong hybridization between the O and As atoms, see Fig. 9. We found that the p states of the As_1 and As_2 atoms changed in comparison to their non-adsorbed states. Although the changes of the the electronic states of As_1 and As_2 in the PDOS were smaller than the changes calculated for the adsorption on a single As_1 atom, our results are still in line with the observed electron transfers. Our results demonstrate that the OH fragments form stable chemisorption modes with nearby As sites. Similar to the interaction with the single As site, the adsorption of H atoms has minimal impact on the electronic properties of the majority of the surface atoms, causing only slight changes of PDOS bands and energies and confirming that these are physisorption modes.

The changes in the electronic density of states of the p orbitals of the O atom after adsorption at the Fe site show hybridisation with the cation (Fig. 10). Similarly, the shifts of the electronic density of states of the As_1 and As_2 atoms after interaction at the two nearby As sites are also almost identical after adsorption at the single As site. The main difference is the larger change in the As-p state than in the Fe-d state due to hybridisation with the O-p orbitals. Finally, we found that the physisorption modes have no impact on the density of states of the H atoms interacting with the surface.

4. Conclusions

In this study, we have reported the chemical oxidation behavior of the arsenopyrite surface in H_2O_2 solutions of varying concentrations, as well as identified the oxidation products. Using froth flotation recovery and contact angle, it was possible to analyze how the wettability of the arsenopyrite surface changed for different levels of oxidation. AFM images showed both the accumulation of oxidation products and changes in the surface morphology of arsenopyrite. We have used XPS spectroscopy to determine changes in the oxidation states of the surface atoms of arsenopyrite, whereas DFT calculations have been employed to determine the H_2O_2 adsorption geometries and changes in the electronic

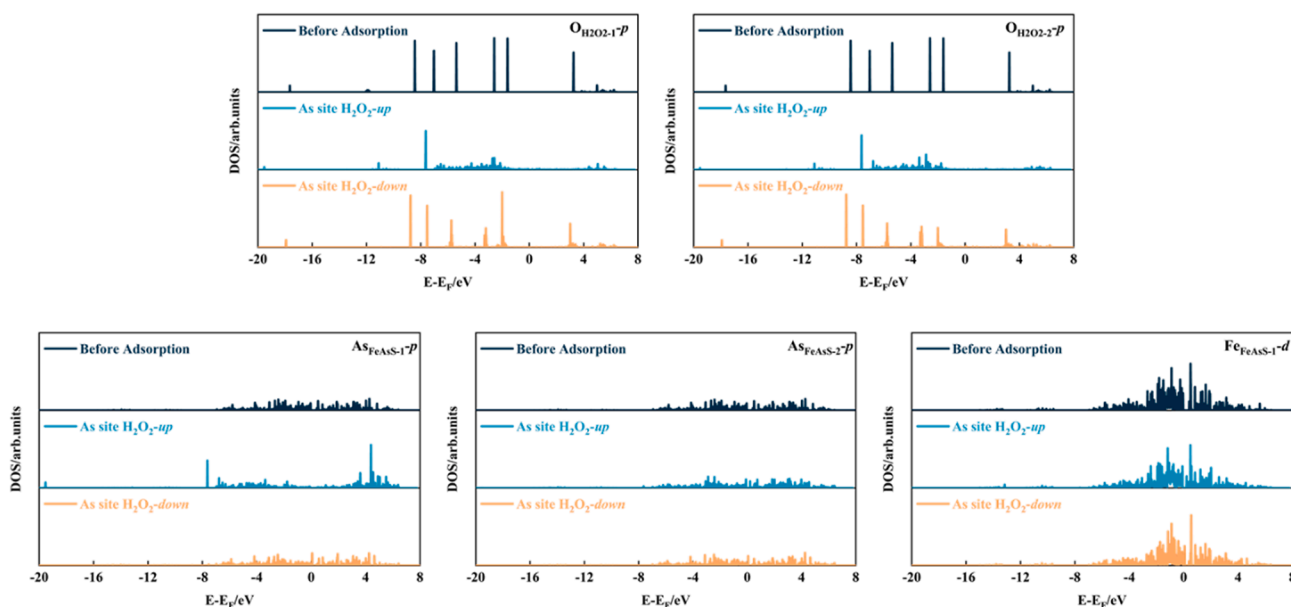


Fig. 8. PDOS of O atoms in the hydrogen peroxide and the interacting Fe and As atoms on the surface (as shown in Fig. 7) in the two adsorption forms of H_2O_2 at a single As site.

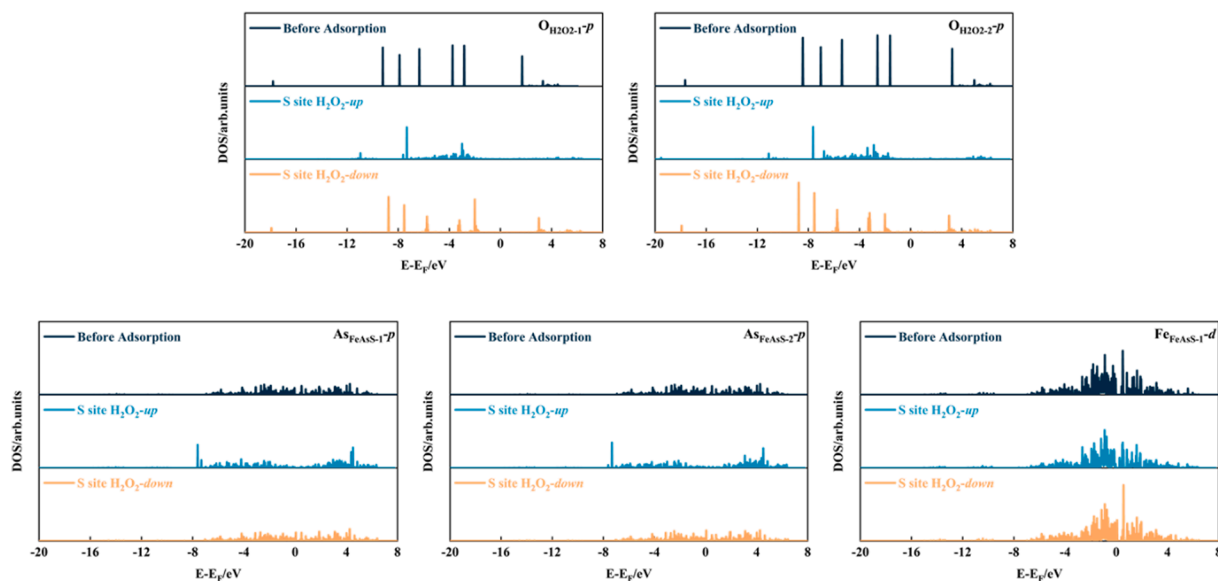


Fig. 9. PDOS of O atoms in the hydrogen peroxide and the interacting Fe and As atoms on the surface (as shown in Fig. 7) in the two adsorption forms of H_2O_2 at two nearby As sites.

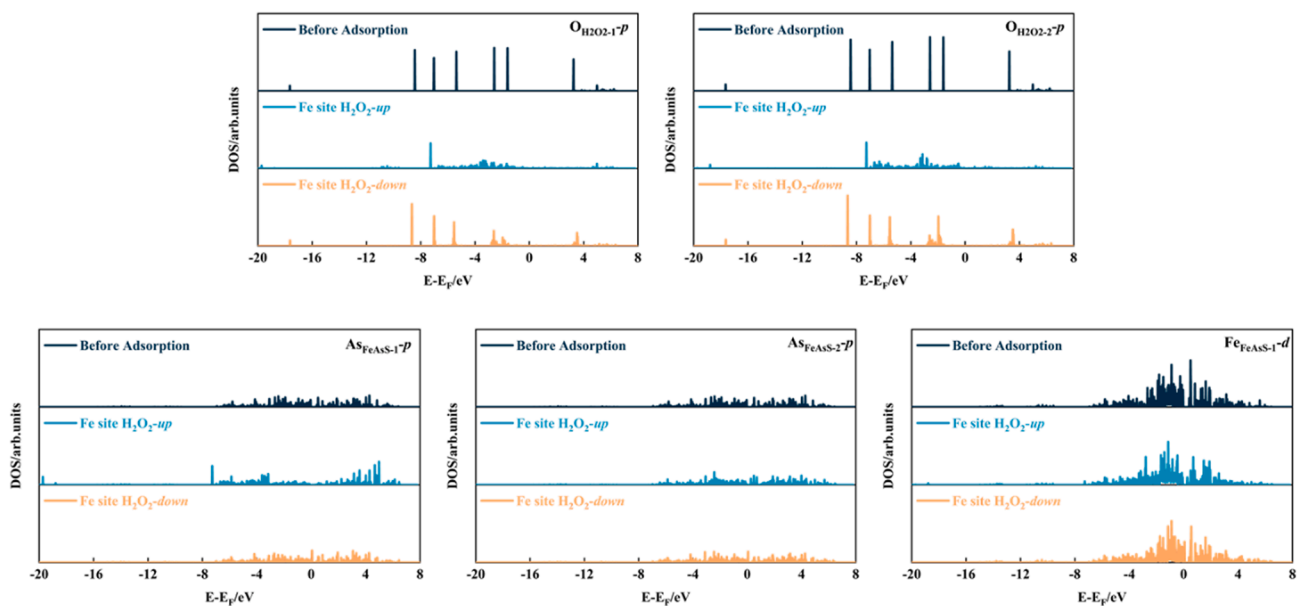


Fig. 10. PDOS of O atoms in the hydrogen peroxide and the interacting Fe and As atoms on the surface (as shown in Fig. 7) in the two adsorption forms of H_2O_2 at two nearby Fe and As site.

properties of the arsenopyrite surface.

The main conclusions of this investigation are summarised below.

- (1) The froth flotation recovery results demonstrate that hydrophilic species are clearly formed on the arsenopyrite surfaces during oxidation, limiting the capacity of the mineral to float. The contact angle measurements also indicate a consistent increase of the surface hydrophilicity as the hydrogen peroxide concentration increases.
- (2) The AFM images demonstrate that oxidation products accumulate and grow, covering the surfaces of the arsenopyrite, following the reaction of this mineral phase with solutions containing an increasing concentration of H_2O_2 . XPS experiments show that surface Fe and S atoms undergo continuous oxidation,

becoming Fe(III) and SO_4^{2-} , respectively, whereas As undergoes stepwise oxidation to As(III) and subsequently to As(V).

- (3) DFT calculations clearly show that the orientation of the hydrogen and oxygen atoms of the H_2O_2 molecule has a substantial impact on the adsorption energies. The H_2O_2 molecule adsorbs physically via its H atoms onto the arsenopyrite surface, whereas the interaction through the O atoms leads to stable chemisorption modes. The most stable adsorption mode of the H_2O_2 molecule is formed by the O atoms coordinating two As atoms of the arsenopyrite surfaces.

The findings presented in this paper provide new information to enhance our understanding of the oxidation process of arsenopyrite in ambient conditions and they assist in opening a real possibility for the exploitation of arsenopyrite-containing gold tailings.

CRedit authorship contribution statement

Kai Jiang: Methodology, Writing – original draft. **David Santos-Carballal:** Methodology, Writing – review & editing. **Jie Liu:** Investigation, Validation. **Yuexin Han:** Writing – review & editing. **Yimin Zhu:** Writing – review & editing. **Yan Wang:** Data curation. **Deju Zhang:** Writing – review & editing. **Nora H. de Leeuw:** Writing – review & editing.

Declaration of Competing Interest

The authors declare that they have no known competing financial interests or personal relationships that could have appeared to influence the work reported in this paper.

Data availability

All data created during this research are provided in full in the results section of this paper.

Acknowledgements

The authors are grateful for the funding provided by the National Natural Science Foundation of China (Grant No. 52104248), the China Postdoctoral Science Foundation (Grant No. 2021M700724), and Postdoctoral Foundation of Northeastern University (Grant No. 20210204). Kai Jiang would like to thank the China Scholarship Council for an Overseas Research Scholarship and the Basic Research Operations Fund (N180106001) provided by the Northeastern University (China) for financial support. Kai Jiang is grateful to Cardiff University for support through a research scholarship from the School of Chemistry. This work used the Supercomputing Facilities at Cardiff University operated by the Advanced Research Computing @ Cardiff (ARCCA) Division on behalf of the Supercomputing Wales (SCW) project, which is part-funded by the European Regional Development Fund (ERDF) via the Welsh Government. For the purpose of Open Access, the author has applied a CC BY public copyright licence to any Author Accepted Manuscript version arising from this submission.

References

- B. Chen, L. Pang, Z. Zhou, Q. Chang, P. Fu, Study on the activation mechanism and hydration properties of gold tailings activated by mechanical-chemical-thermal coupling, *J. Build. Eng.* 48 (2022), 104014, <https://doi.org/10.1016/j.job.2022.104014>.
- T. Norgate, N. Haque, Using life cycle assessment to evaluate some environmental impacts of gold production, *J. Clean. Prod.* 29–30 (2012) 53–63, <https://doi.org/10.1016/j.jclepro.2012.01.042>.
- G.M. Ritcey, Tailings management in gold plants, *Hydrometallurgy* 78 (2005) 3–20, <https://doi.org/10.1016/j.hydromet.2005.01.001>.
- Y. Kim, M. Kim, J. Sohn, H. Park, Applicability of gold tailings, waste limestone, red mud, and ferronickel slag for producing glass fibers, *J. Clean. Prod.* 203 (2018) 957–965, <https://doi.org/10.1016/j.jclepro.2018.08.230>.
- H. Lin, X. Jiang, B. Li, Y. Dong, L. Qian, Soilless revegetation: an efficient means of improving physicochemical properties and reshaping microbial communities of high-salty gold mine tailings, *Ecotoxicol. Environ. Saf.* 207 (2021), 111246, <https://doi.org/10.1016/j.ecoenv.2020.111246>.
- Z. Wei, J. Zhao, W. Wang, Y. Yang, S. Zhuang, T. Lu, Z. Hou, Utilizing gold mine tailings to produce sintered bricks, *Constr. Build. Mater.* 282 (2021), 122655, <https://doi.org/10.1016/j.conbuildmat.2021.122655>.
- J.N. Wang, R. Yu, W.Y. Xu, C.Y. Hu, Z.H. Shui, D. Qian, Y. Leng, K.N. Liu, D.S. Hou, X.P. Wang, A novel design of low carbon footprint Ultra-High Performance Concrete (UHPC) based on full scale recycling of gold tailings, *Constr. Build. Mater.* 304 (2021) 124664, <https://doi.org/10.1016/j.conbuildmat.2021.124664>.
- C. Zhang, X. Wang, S. Jiang, M. Zhou, F. Li, X. Bi, S. Xie, J. Liu, Heavy metal pollution caused by cyanide gold leaching: a case study of gold tailings in central China, *Environ. Sci. Pollut. Res.* 28 (2021) 29231–29240, <https://doi.org/10.1007/s11356-021-12728-w>.
- H. Qin, X. Guo, Q. Tian, L. Zhang, Pyrite enhanced chlorination roasting and its efficacy in gold and silver recovery from gold tailing, *Sep. Purif. Technol.* 250 (2020), 117168, <https://doi.org/10.1016/j.seppur.2020.117168>.
- C. Manjiao, Z. Zhengfu, H. Xinjun, T. Jianping, W. Jingsong, W. Rundong, Z. Xian, Z. Xinjun, S. Peilun, L. Dianwen, Oxidation mechanism of the arsenopyrite surface by oxygen with and without water: experimental and theoretical analysis, *Appl. Surf. Sci.* 573 (2022), 151574, <https://doi.org/10.1016/j.apsusc.2021.151574>.
- X.u. Zhang, Y.-l. Feng, H.-R. Li, Enhancement of bio-oxidation of refractory arsenopyritic gold ore by adding pyrolusite in bioleaching system, *Trans. Nonferrous Met. Soc. Chin.* 26 (9) (2016) 2479–2484, [https://doi.org/10.1016/S1003-6326\(16\)64339-X](https://doi.org/10.1016/S1003-6326(16)64339-X).
- A. Seitkan, S.A.T. Redfern, Processing double refractory gold-arsenic-bearing concentrates by direct reductive melting, *Miner. Eng.* 98 (2016) 286–302, <https://doi.org/10.1016/j.mineng.2016.08.017>.
- P.N. Neingo, T. Tholana, Trends in productivity in the South African gold mining industry, *J. South Afr. Inst. Min. Metall.* 116 (2016) 283–290, <https://doi.org/10.17159/2411-9717/2016/v116n3a10>.
- A. Murciego, E. Álvarez-Ayuso, S.C. Aldana-Martínez, A. Sanz-Arranz, J. Medina-García, F. Rull-Pérez, P. Villar-Alonso, Characterization of secondary products in arsenopyrite-bearing mine wastes: influence of cementation on arsenic attenuation, *J. Hazard. Mater.* 373 (2019) 425–436, <https://doi.org/10.1016/j.jhazmat.2019.03.086>.
- S.L. DeSisto, H.E. Jamieson, M.B. Parsons, Influence of hardpan layers on arsenic mobility in historical gold mine tailings, *Appl. Geochem.* 26 (2011) 2004–2018, <https://doi.org/10.1016/j.apgeochem.2011.06.030>.
- B.G. Lottermoser, P.M. Ashley, Mobility and retention of trace elements in hardpan-cemented cassiterite tailings, north Queensland, Australia, *Environ. Geol.* 50 (2006) 835–846, <https://doi.org/10.1007/s00254-006-0255-8>.
- K. Jiang, J. Liu, Y. Wang, D. Zhang, Y. Han, Surface properties and flotation inhibition mechanism of air oxidation on pyrite and arsenopyrite, *Appl. Surf. Sci.* 610 (2023), 155476, <https://doi.org/10.1016/j.apsusc.2022.155476>.
- C.L. Corkhill, D.J. Vaughan, Arsenopyrite oxidation - a review, *Appl. Geochem.* 24 (2009) 2342–2361, <https://doi.org/10.1016/j.apgeochem.2009.09.008>.
- T. Zhu, X. Lu, H. Liu, J. Li, X. Zhu, J. Lu, R. Wang, Quantitative X-ray photoelectron spectroscopy-based depth profiling of bioleached arsenopyrite surface by *Acidithiobacillus ferrooxidans*, *Geochim. Cosmochim. Acta* 127 (2014) 120–139, <https://doi.org/10.1016/j.gca.2013.11.025>.
- M.T. Emett, G.H. Khoe, Photochemical oxidation of arsenic by oxygen and iron in acidic solutions, *Water Res.* 35 (2001) 649–656, [https://doi.org/10.1016/S0043-1354\(00\)00294-3](https://doi.org/10.1016/S0043-1354(00)00294-3).
- J. Ryu, D. Monllor-Satoca, D.H. Kim, J. Yeo, W. Choi, Photooxidation of arsenite under 254 nm irradiation with a quantum yield higher than unity, *Environ. Sci. Tech.* 47 (2013) 9381–9387, <https://doi.org/10.1021/es402011g>.
- Y. Wang, J. Xu, J. Li, F. Wu, Natural montmorillonite induced photooxidation of As (III) in aqueous suspensions: roles and sources of hydroxyl and hydroperoxyl/superoxide radicals, *Journal of Hazardous Materials.* 260 (2013) 255–262, <https://doi.org/10.1016/j.jhazmat.2013.05.028>.
- G. Kresse, J. Furthmüller, Efficiency of ab-initio total energy calculations for metals and semiconductors using a plane-wave basis set, *Comput. Mater. Sci* 6 (1996) 15–50, [https://doi.org/10.1016/0927-0256\(96\)00008-0](https://doi.org/10.1016/0927-0256(96)00008-0).
- G. Kresse, Ab initio molecular dynamics for liquid metals, *J. Non Cryst. Solids* 192–193 (1995) 222–229, [https://doi.org/10.1016/0022-3093\(95\)00355-X](https://doi.org/10.1016/0022-3093(95)00355-X).
- P.E. Blöchl, Projector augmented-wave method, *Phys. Rev. B* 50 (1994) 17953–17979, <https://doi.org/10.1103/PhysRevB.50.17953>.
- J.P. Perdew, K. Burke, M. Ernzerhof, Generalized gradient approximation made simple, *Phys. Rev. Lett.* 77 (1996) 3865–3868, <https://doi.org/10.1103/PhysRevLett.77.3865>.
- S. Grimme, J. Antony, S. Ehrlich, H. Krieg, A consistent and accurate ab initio parametrization of density functional dispersion correction (DFT-D) for the 94 elements H-Pu, *J. Chem. Phys.* 132 (2010) 154104, <https://doi.org/10.1063/1.3382344>.
- N.Y. Dzade, N.H. De Leeuw, Periodic DFT + U investigation of the bulk and surface properties of marcasite (FeS₂), *Phys. Chem. Chem. Phys.* 19 (2017) 27478–27488, <https://doi.org/10.1039/c7cp04413e>.
- G.W. Watson, E.T. Kelsey, N.H. De Leeuw, D.J. Harris, S.C. Parker, Atomistic simulation of dislocations, surfaces and interfaces in MgO, *J. Chem. Soc. - Faraday Trans.* 92 (1996) 433–438, <https://doi.org/10.1039/f9969200433>.
- H.W. Nesbitt, Oxidation states and speciation of secondary products on pyrite and arsenopyrite reacted with mine waste waters and air, *Mineral. Petrol.* 62 (1998) 123–144, <https://doi.org/10.1007/BF01173766>.
- H.W. Nesbitt, I.J. Muir, A.R. Prarr, Oxidation of arsenopyrite by air and air-saturated, distilled water, and implications for mechanism of oxidation, *Geochim. Cosmochim. Acta.* 59 (1995) 1773–1786, [https://doi.org/10.1016/0016-7037\(95\)00081-A](https://doi.org/10.1016/0016-7037(95)00081-A).
- A.N. Buckley, G.W. Walker, The surface composition of arsenopyrite exposed to oxidizing environments, *Appl. Surf. Sci.* 35 (1988) 227–240, [https://doi.org/10.1016/0169-4332\(88\)90052-9](https://doi.org/10.1016/0169-4332(88)90052-9).
- C.L. Corkhill, P.L. Wincott, J.R. Lloyd, D.J. Vaughan, The oxidative dissolution of arsenopyrite (FeAsS) and enargite (Cu₃AsS₄) by *Leptospirillum ferrooxidans*, *Geochim. Cosmochim. Acta* 72 (2008) 5616–5633, <https://doi.org/10.1016/j.gca.2008.09.008>.
- M. Chen, Z. Zhang, X. Hu, J. Tian, Z. Lu, J. Wang, R. Wan, X. Zhou, X. Zhou, P. L. Shen, D. Liu, Oxidation mechanism of arsenopyrite under alkaline conditions: experimental and theoretical analyses, *J. Clean. Prod.* 358 (2022), 131987, <https://doi.org/10.1016/j.jclepro.2022.131987>.
- A.N.G.S. Chaufuss, H.W.A.N. Esbitt, M.I.J.S. Caini, H.A.H. Oechst, M.I.G. B. Ancroft, R.Ü.S. Zargan, *Schaufuss* 2000 (85) (2000) 1754–1766.
- M.C. Costa, A.M. Botelho, L.M. Abrantes, Characterization of a natural and an electro-oxidized arsenopyrite: a study on electrochemical and X-ray photoelectron spectroscopy, *Int. J. Miner. Process.* 65 (2002) 83–108, [https://doi.org/10.1016/S0301-7516\(01\)00059-X](https://doi.org/10.1016/S0301-7516(01)00059-X).

- [37] Y.L. Mikhlin, A.S. Romanchenko, I.P. Asanov, Oxidation of arsenopyrite and deposition of gold on the oxidized surfaces: a scanning probe microscopy, tunneling spectroscopy and XPS study, *Geochim. Cosmochim. Acta* 70 (2006) 4874–4888, <https://doi.org/10.1016/j.gca.2006.07.021>.
- [38] S. Richardson, D.J. Vaughan, Arsenopyrite: a spectroscopic investigation of altered surfaces, *Mineral. Mag.* 53 (1989) 223–229, <https://doi.org/10.1180/minmag.1989.053.370.09>.
- [39] P. Zhang, W. Huang, Z. Ji, C. Zhou, S. Yuan, Mechanisms of hydroxyl radicals production from pyrite oxidation by hydrogen peroxide: surface versus aqueous reactions, *Geochim. Cosmochim. Acta* 238 (2018) 394–410, <https://doi.org/10.1016/j.gca.2018.07.018>.
- [40] D. Santos-Carballal, A. Cadi-Essadek, N.H. de Leeuw, Catalytic conversion of CO and H₂ into Hydrocarbons on the cobalt Co(111) surface: implications for the Fischer-Tropsch process, *J. Phys. Chem. C* 125 (2021) 11891–11903, <https://doi.org/10.1021/acs.jpcc.1c00254>.
- [41] G. Henkelman, A. Arnaldsson, H. Jónsson, A fast and robust algorithm for Bader decomposition of charge density, *Comput. Mater. Sci.* 36 (2006) 354–360, <https://doi.org/10.1016/j.commatsci.2005.04.010>.
- [42] N.Y. Dzade, A. Roldan, N.H. De Leeuw, Structures and properties of As(OH)₃ adsorption complexes on hydrated mackinawite (FeS) surfaces: a DFT - D2 study, *Environ. Sci. Tech.* 51 (2017) 3461–3470, <https://doi.org/10.1021/acs.est.7b00107>.